2013

Arrays Fabrication and Photoelectrochemical Properties of Sn-doped Vertically Oriented Hematite Nanorods for Solar Cells

Chunting Liu

Hongzhou Dong

Qian Zhang

Qiong Sun

Liyan Yu

See next page for additional authors

Recommended Citation

Liu, Chunting, Hongzhou Dong, Qian Zhang, Qiong Sun, Liyan Yu, and Lifeng Dong. "Array fabrication and photoelectrochemical properties of Sn-doped vertically oriented hematite nanorods for solar cells." Journal of Renewable and Sustainable Energy 5, no. 2 (2013): 021416.

Array fabrication and photoelectrochemical properties of Sn-doped vertically oriented hematite nanorods for solar cells

Chunting Liu (刘春廷),[1] Hongzhou Dong (董红周),[1] Qian Zhang (张乾),[1] Qiong Sun (孙琼),[1] Liyan Yu (于立岩),[1] and Lifeng Dong (董立峰)[1,2,a)]
[1]*College of Materials Science and Engineering, Qingdao University of Science and Technology, Qingdao 266042, People's Republic of China*
[2]*Department of Physics, Astronomy, and Materials Science, Missouri State University, Springfield, Missouri 65897, USA*

(Received 28 August 2012; accepted 1 February 2013; published online 29 March 2013)

We report on the synthesis and characterization of Sn-doped hematite nanorods as well as their implementation as the photoanode for solar cells. Hematite nanorods are prepared on fluorine-doped tin oxide (FTO) substrates by a hydrothermal method, followed by a two-step sintering in air, and Sn-doping is achieved by adding $SnCl_4$ into the mixture solution during the hydrothermal process. In comparison to un-doped hematite, Sn-doped hematite nanorods exhibit a higher array growth density along the direction [110], which indicates that the Sn-doping can facilitate the vertically oriented growth of the hematite nanorod arrays; moreover, the Sn-doping can result in enhanced photocurrent density and photoelectrical efficiency due to the improved carrier density. These new findings will provide new information to enhance the photoelectrochemical characteristics of hematite, one of the best potential photoanode materials. © *2013 American Institute of Physics*. [http://dx.doi.org/10.1063/1.4798431]

I. INTRODUCTION

Photovoltaic is a promising renewable energy technology that converts sunlight to electricity. Although silicon-based photovoltaic devices are commercially available, their photovoltaic devices continue to face a number of challenges, including the cost of silicon materials, the efficiency of energy conversion, and long-term stability. Hematite (α-Fe_2O_3) is an intrinsic n-type semiconductor with an indirect band-gap of 2.1 eV.[1] This theoretically allows the usage of approximately 40% of solar spectrum, which is significantly more than other wide band-gap semiconductors, such as TiO_2.[2] Combined with its electrochemical stability, low toxicity, wide abundance, and low-cost, hematite is a desirable photoanode material for potential applications in photoelectrochemical (PEC) solar cells.[3] Additionally, hematite has been investigated for applications in gas sensor,[4] field emission,[5] heterogeneous catalysis,[6] and lithium-ion battery.[7] However, the photoelectrochemical activity of hematite can be limited by several factors, such as low conductivity, low optical absorption coefficient,[8] very short excited-state lifetime ($\sim 10^{-12}$ s),[9] poor oxygen evolution reaction kinetics,[10] high electron-hole recombination rate, and short hole diffusion length (2–4 nm).[11] To address these limitations and optimize energy conversion efficiency, enormous efforts have been focused on the development of hematite nanostructures and the modification of their electronic structure via elemental doping. One potential solution to the traditional problems associated with bulk α-Fe_2O_3 is to use high aspect ratio one-dimensional (1-D) nanostructures as the photoelectrode.[12,13] In this configuration, light absorption occurs along the longitudinal dimension of the nanostructures, while carrier separation occurs by the diffusion across the lateral radial dimension. Hematite structures have also

a)Author to whom correspondence should be addressed. Electronic mail: DongLifeng@qust.edu.cn.

been doped with different elements to improve their efficiency, such as Si, Ti, Al, Mg, Zn, Cr, Mo, and Pt.[14–17] However, very little is known about the photoelectrochemical properties of Sn-doped α-Fe_2O_3 nanorods.

In this study, hematite nanorods were directly formed on fluorine-doped tin oxide (FTO) substrates by a hydrothermal method, followed by a two-step sintering in air, and Sn-doping was achieved with the addition of $SnCl_4$ into the mixture solution during the hydrothermal process. The morphology and crystal structures of un-doped and Sn-doped hematite nanorod arrays were characterized, and their photoelectrochemical properties were comparatively investigated.

II. SYNTHESIS AND CHARACTERIZATION METHODS

A. Synthesis of hematite nanostructures and their photoanodes

Hematite nanorods were fabricated on FTO glass substrates by hydrothermal treatment of a mixture of $FeCl_3$ and $NaNO_3$ solutions.[18] In a typical experimental procedure, 0.15 M ferric chloride ($FeCl_3 \cdot 6H_2O$) and 1.0 M sodium nitrate ($NaNO_3$) were dissolved in a 20 ml solution of 1.5 vol. % HCl (36.5%–38%) and ethanol in a volume ratio of 3:7. After stirring for 10 min, the mixture solution was transferred into a Teflon-lined stainless-steel autoclave of 40 ml capacity. A piece of FTO glass slide, washed with acetone, ethanol, and then deionized water was put into the autoclave and heated at 100 °C for 4 h. A uniform layer of iron oxyhydroxide (FeOOH) film (yellow color) was formed on the FTO substrates. The FeOOH coated substrates were then washed with deionized water to remove any residual salt and subsequently sintered in air at 500 °C for 2 h. During the sintering process, the FeOOH nanorods were converted into hematite nanorods. For photoelectrochemical measurements, hematite nanorods were annealed at 800 °C for 20 min. Sn-doped hematite was prepared by the same procedure as un-doped hematite nanorods, except that 1 ml of tin (IV) chloride ($SnCl_4$) ethanol solution (20 mg/ml) was added into the solution mixture as tin precursor. Hematite nanostructures were fashioned into a photoanode by securing a copper wire onto a bare portion of FTO substrates by soldering. The substrates were then sealed on all edges with epoxy resin except for a working area of 0.12 cm^2.

B. Characterization

Hematite nanostructured films on FTO substrates were characterized with a powder X-ray diffractometer (XRD, Rigaku D/max-rA) equipped with a rotating anode and a Cu Kα1 radiation source ($\lambda = 1.5406$ Å). Diffraction patterns were recorded from 20° to 70° with a step size of 0.04° at 1°/min. The morphology of the nanostructures was characterized with a field emission scanning electron microscope (FESEM, JEOL JSM-6700F). Photoelectrochemical measurements were recorded by an electrochemical workstation (CHI 660D, CH instruments, Inc.) using a three-electrode configuration with the hematite film as the working electrode, Ag/AgCl as the reference electrode, and platinum foil as the counter electrode in 1 M NaOH solution. Sunlight was simulated with a 150 W Xenon lamp and an AM 1.5 G air mass filter (Newport, 96000 Full Spectrum Solar Simulator). External quantum efficiency (EQE) was evaluated by a testing system consisting of a xenon lamp (300 W, Model 6258, Newport), a cornerstone 260 monochromator (Model 74125, Newport), a UV silicon detector (Model 70356, Newport), a Newport chopper (Model 75151), a dual channel RS232 Merlin radiometry system (Models 70100 thru 70105, Newport), and an Oriel amplifier for QE light bias.

III. RESULTS AND DISCUSSION

As given in Fig. 1, both un-doped and Sn-doped products were covered with a red film of hematite nanorods, and the Sn-doped sample exhibited a higher growth density of vertically oriented nanorod arrays with a length of 400–600 nm and a diameter of 20–30 nm at the tip and 80–100 nm at the bottom (Fig. 1(b)). This indicates that Sn-doping facilitates the growth of vertically oriented hematite nanorod arrays on FTO substrates.

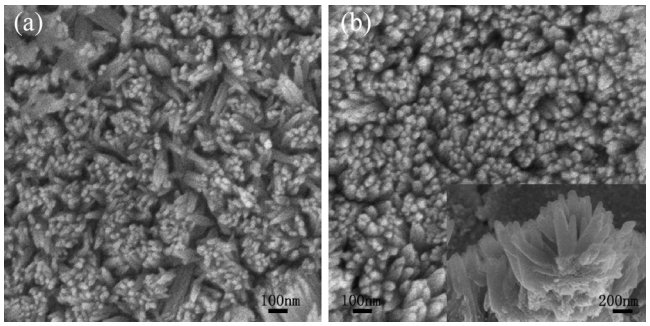

FIG. 1. SEM images of (a) un-doped and (b) Sn-doped hematite nanorod films on the FTO substrates. [Inset is the cross-sectional microstructure in Fig. 1(b)].

In order to identify the structures of the reaction products, XRD data were obtained from FTO substrate, un-doped and Sn-doped hematite nanorod films on the FTO substrates. The FTO substrate was confirmed to be SnO_2 (JCPDS card number 41-1445, Fig. 2(a)). As shown in Figs. 2(b) and 2(c), hematite α-Fe_2O_3 (JCPDS card number 33-0664) and SnO_2 (JCPDS card number 41-1445) were confirmed for both un-doped and Sn-doped hematite nanorod arrays, and no other crystal phase was observed. Both arrays display similar XRD patterns with a prominent (110) diffraction peak, which has been suggested as the preferential direction for electron transport in hematite.[18] The [110] direction provides an excellent path for the diffusion of electrons because of the strongly anisotropic conductivity of hematite. The conduction along the [001] direction in hematite, which follows a site hopping mechanism, is four orders of magnitude lower than other directions perpendicular to (100) plane, which contains the [110] direction.[14] In Fig. 2(b), the thermally stable phase α-Fe_2O_3 was obtained with several weak reflections corresponding to the (104), (024), (116), (122), and (300) planes besides the dominant (110) reflection, which suggests the existence of multiple orientations in hematite nanostructures. However, there is only (110) hematite diffraction peak in Fig. 2(c), indicating that Sn-doping facilitates vertical growth of hematite nanorods on the FTO substrate, consistent with the FESEM characterizations above.

The testing configuration and photoelectrochemical performance for un-doped and Sn-doped hematite nanorod films are shown in Fig. 3(a). As shown in Fig. 3(b), in the dark, both

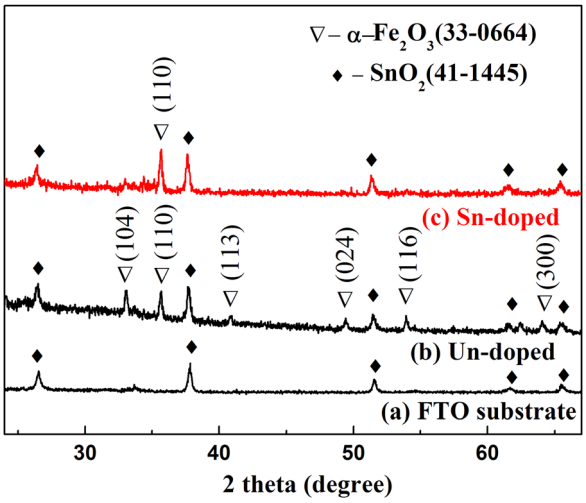

FIG. 2. XRD spectra collected for (a) FTO substrate, (b) un-doped, and (c) Sn-doped hematite nanorods films on the FTO substrates.

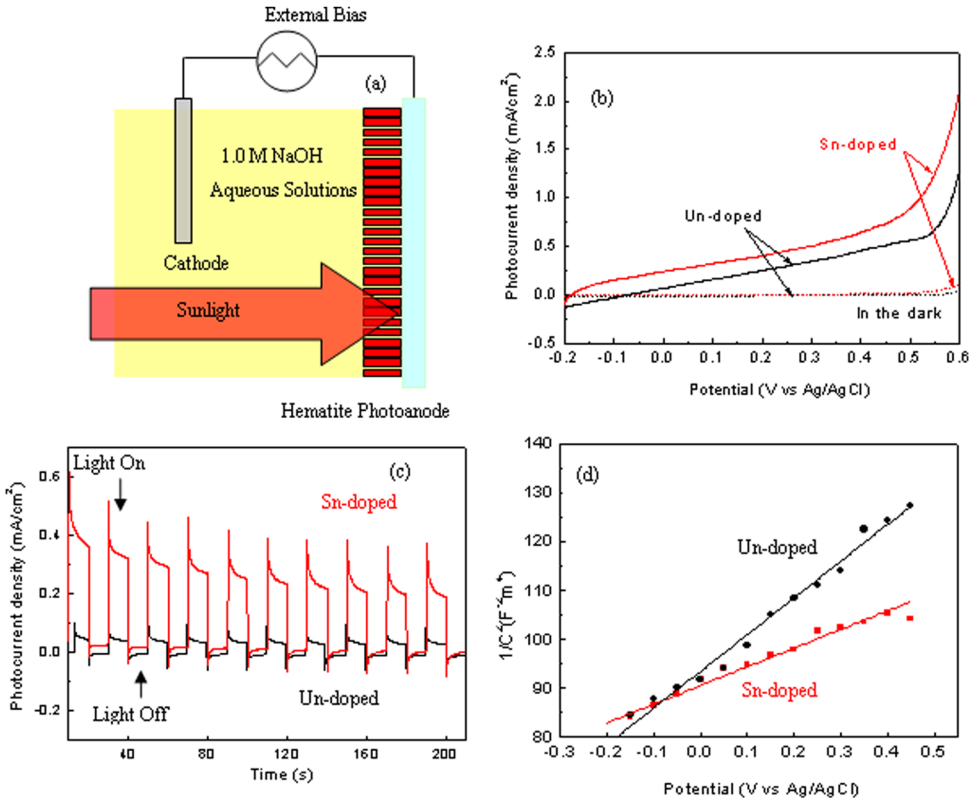

FIG. 3. (a) Testing configuration, (b) photocurrent density *vs.* potential curves, (c) photocurrent-transient responses measured during cycling operation, and (d) Mott-Schottky plots in the dark at a frequency of 10 kHz for hematite nanorod array films.

the samples with and without Sn-doping display a negligible response with a very small saturation photocurrent density (0.099 and 0.081 mA/cm^2 at 0.6 V vs. Ag/AgCl, respectively). Under the illumination, the photocurrent density of 1.20 mA/cm^2 at 0.60 V vs. Ag/AgCl was observed for those un-doped hematite nanorods, and the optoelectronic response was further enhanced to 2.03 mA/cm^2 at 0.60 V vs. Ag/AgCl when the hematite film was incorporated with Sn [red curve in Fig. 3(b)], suggesting a correlation between Sn-doping and photocurrent density of hematite nanorod arrays. Sn-doped α-Fe_2O_3 nanorods exhibited higher photocurrent density than those non-doped hematite films. Consequently, we carried out a photo-current-transient response study [Fig. 3(c)], which was done by periodically chopping the light at a constant potential of 0.1 V. The photocurrent density of the Sn-doped hematite was higher than that of un-doped films. On turning on the light, we obtained photo-current-transient spikes in the upward direction, which then decayed from a peak to a steady state. On turning the light off after 10 s of illumination, the photocurrent dropped towards zero and reverted back again when the light was turned back on. This falling photo-current-transient decay is an indication of a rapid removal of conduction-band electrons into the bulk,[19] and the spike-like transient response is caused by a "back reaction," or a recombination of the photogenerated electrons and holes with the surface states.[20]

According to the Mott-Schottky equation, the slope of the plots in Fig. 3(d) has an inverse relationship with the carrier density of semiconductor film,

$$N_d = (2/e_0\varepsilon\varepsilon_0)[d(1/C^2)/dV]^{-1}, \quad (1)$$

where C is specific capacitance (F/cm^2), e_0 is electron charge, ε is dielectric constant of hematite, ε_0 is the permittivity of vacuum, N_d is carrier density, and V is the applied potential on

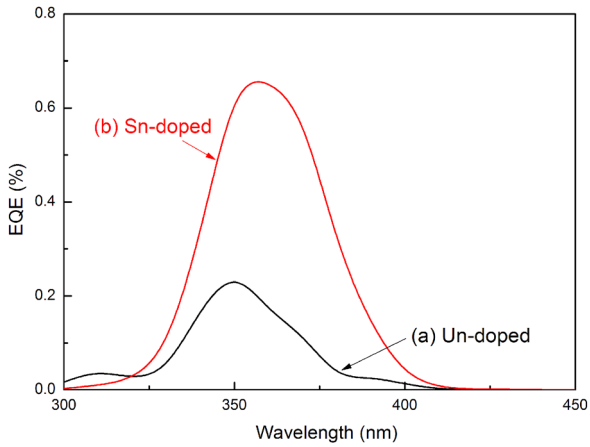

FIG. 4. External quantum efficiency of (a) un-doped and (b) Sn-doped hematite nanorod films on the FTO substrates.

electrode. Positive slopes indicate that un-doped and Sn-doped hematite nanorod arrays are n-type semiconductors, as shown in Fig. 3(d). The slopes determined from the analysis of Mott-Schottky plots were used to estimate carrier densities. With an ε value of 80 for hematite,[8] carrier densities of un-doped and Sn-doped hematite nanorods were calculated to be 8.6×10^{19} and $1.5 \times 10^{20}\,\mathrm{cm}^{-3}$, respectively. The differences in the photoelectrochemical performance between the un-doped and Sn-doped electrodes can be related to the Sn incorporation. A recent density functional theory (DFT) calculation on Al^{3+} doped Fe_2O_3 indicates that a contraction of the hematite lattice can enhance the polaronic conductivity of hematite by improving the rate of carrier hopping between cations.[21] In this study, the photocurrent enhancement by the substitution of Sn^{4+} for Fe^{3+} can result from the improvement of carrier density and electron transport in the hematite α-Fe_2O_3, which may be carried out by a polaron hopping mechanism and electron hopping from Fe^{2+} to Fe^{3+} sites via thermal activation rather than by free conduction. Enhanced current in the dark for Sn-doped hematite was observed (Fig. 3(b)), indicating that the charge compensation of incorporated Sn^{4+} via the reduction of additional Fe^{3+} species to Fe^{2+} can increase the n-type conductivity of α-Fe_2O_3 single crystals and films.[22]

Fig. 4 shows the external quantum efficiency of un-doped and Sn-doped hematite nanorod films on the FTO substrates, measured with a 0.1 V bias. A peak EQE value was 0.66% at 356 nm for Sn-doped hematite nanorod films, which is nearly three times that of un-doped hematite nanorods with 0.23% at 349 nm. This clearly demonstrates that Sn-doping can effectively increase photoelectrical conversion efficiency. More study is underway to optimize the concentration of Sn-doping and to investigate the interfaces between hematite and Sn-dopant.

IV. CONCLUSIONS

Experimental results clearly demonstrate that hematite nanorod arrays can be directly synthesized on conductive FTO substrates by a simple hydrothermal method, and Sn-doping can be achieved with the addition of $SnCl_4$ into the mixture solution during the hydrothermal process. Sn-doping can enhance the vertical-orientation of hematite nanorods to the FTO substrates and can increase carrier density. Therefore, in comparison to un-doped hematite nanorods, Sn-doped hematite nanorods demonstrated higher photocurrent densities and external quantum efficiency.

ACKNOWLEDGMENTS

This work was partially supported by the International Science & Technology Cooperation Program of China (S2013ZR0296), the National Natural Science Foundation of China (51172113), the Shandong Natural Science Foundation for Distinguished Young Scholars (JQ201118), the Taishan Overseas Scholar program from the Shandong Province Government, P.R. China, the

Qingdao Municipal Science and Technology Commission (12-1-4-136-hz), and the Faculty Research Grant and the Sabbatical Leave Award from Missouri State University.

[1]B. Gilbert, C. Frandsen, E. R. Maxey, and D. M. Sherman, Phys. Rev. B **79**, 035108 (2009); K. Sivula, F. Le Formal, and M. Grätzel, ChemSusChem. **4**, 432 (2011).
[2]M. Grätzel, Nature **414**, 338 (2001); A. Kudo and Y. Miseki, Chem. Soc. Rev. **38**, 253 (2009); R. van de Krol, Y. Liang, and J. Schoonman, J. Mater. Chem. **18**, 2311 (2008).
[3]P. Hiralal, S. Saremi-Yarahmadi, B. C. Bayer, H. Wang, S. Hofmann, K. G. Upul Wijayantha, and G. A. J. Amaratunga, Sol. Energy Mater. Sol. Cells **95**, 1819 (2011).
[4]H. T. Sun, C. Cantalini, M. Faccio, M. Pelino, M. Catalano, and L. Tapfer, J. Am. Ceram. Soc. **79**, 927 (1996).
[5]Y. W. Zhu, T. Yu, C. H. Sow, Y. J. Liu, A. T. S. Wee, X. J. Xu, C. T. Lim, and J. T. L. Thong, Appl. Phys. Lett. **87**, 023103 (2005).
[6]B. C. Faust, M. R. Hoffmann, and D. W. Bahnemann, J. Phys. Chem. **93**, 6371 (1989); S. Y. Lian, E. B. Wang, L. Gao, D. Wu, Y. L. Song, and L. Xu, Mater. Res. Bull. **41**, 1192 (2006).
[7]J. Chen, L. Xu, W. Li, and X. Gou, Adv. Mater. **17**, 582 (2005).
[8]I. Cesar, K. Sivula, A. Kay, R. Zboril, and M. Graetzel, J. Phys. Chem. C **113**, 772 (2009).
[9]N. J. Cherepy, D. B. Liston, J. A. Lovejoy, H. M. Deng, and J. Z. Zhang, J. Phys. Chem. B **102**, 770 (1998).
[10]M. P. Dareedwards, J. B. Goodenough, A. Hamnett, and P. R. Trevellick, J. Chem. Soc., Faraday Trans. 1 **79**, 2027 (1983).
[11]K. Sivula, R. Zboril, F. Le Formal, R. Robert, A. Weidenkaff, J. Tucek, J. Frydrych, and M. Grätzel, J. Am. Chem. Soc. **132**, 7436 (2010).
[12]N. S. Lewis, Science **315**, 798 (2007).
[13]A. Kay, I. Cesar, and M. Grätzel, J. Am. Chem. Soc. **128**, 15714 (2006).
[14]N. Iordanova, M. Dupuis, and K. M. Rosso, J. Chem. Phys. **122**, 144305 (2005).
[15]S. Saremi-Yarahmadi, K. G. U. Wijayantha, A. A. Tahir, and B. Vaidhyanathan, J. Phys. Chem. C **113**, 4768 (2009).
[16]J. Velev, A. Bandyopadhyay, W. H. Butler, and S. J. Sarker, Phys. Rev. B **71**, 205208 (2005).
[17]J. S. Jang, J. Lee, H. Ye, F. R. F. Fan, and A. J. Bard, J. Phys. Chem. C **113**, 6719 (2009).
[18]L. Vayssieres, N. Beermann, S. E. Lindquist, and A. Hagfeldt, Chem. Mater. **13**, 233 (2001).
[19]C. M. Eggleston, A. J. A. Shankle, A. J. Moyer, I. Cesar, and M. Grätzel, Aquat. Sci. **71**, 151 (2009).
[20]A. Watanabe and H. Kozuka, J. Phys. Chem. B **107**, 12713 (2003).
[21]A. Kleiman-Shwarsctein, M. N. Huda, A. Walsh, Y. F. Yan, G. D. Stuckyst, Y. S. Hu, M. M. Al-Jassim, and E. W. McFarland, Chem. Mater. **22**, 510 (2010).
[22]M. Anderman and J. H. Kennedy, in *Semiconductor Electrodes*, edited by H. O. Finklea (Elsevier, Amsterdam, 1988), Chap. 3.